Edinburgh Research Explorer

Effect of Glass Fibre Sizing on the Interfacial Properties of Composites Produced using In-Situ Polymerised Polyamide-6 Transfer Moulding

OPEN ACCESS

Effect of Glass Fibre Sizing on the Interfacial Properties of Composites Produced using In-Situ Polymerised Polyamide-6 Transfer Moulding

James J. Murray[a,c*], Ankur Bajpai[a], James Quinn[a], Jake McClements[a,d], Klaus Gleich[b], Edward D. McCarthy[a], Conchúr M. Ó Brádaigh[a]

[a] School of Engineering, Institute for Materials and Processes, Sanderson Building, The University of Edinburgh, Robert Stevenson Road, EH9 3FB, Scotland, UK

[b] Johns Manville Europe GmbH, Werner-Schuller-Str.1, 97877 Wertheim, Germany

[c] Present address: Athlone Institute of Technology, Dublin Road, Athlone, Co. Westmeath, N37 HD68, Ireland

*Corresponding Author: Email address: j.j.murray@ed.ac.uk

Abstract

The fibre-matrix interfacial properties of glass-fibre/polyamide-6 (GF/PA-6) composites produced by thermoplastic resin transfer moulding (TP-RTM) were investigated. Two different fibre sizings were compared, a specially-developed novel reactive fibre sizing and a standard silane glass fibre sizing. Scanning electron microscopy, atomic force microscopy and a number of mass-loss techniques were employed to study the form, distribution, quantity and degradation temperature of the fibre sizings. Activated PA-6 monomer precursor materials with viscosities of ~10 mPa·s were injected into the glass-fibre fabrics, contained between heated press platens, and polymerisation occurred in-situ within several minutes. Glass-fabric laminates with fibre volume fractions of ~53% and low void content were produced at a pressure of ~4 bar, the low viscosity of the monomer negating the need for expensive high-pressure injection. Similar quality between the laminates was demonstrated by measuring density, thickness, fibre volume fraction, void

content and fibre bundle distribution. Transverse mechanical properties of the composites reinforced with the novel reactive sizing were 20-28% higher than those with the standard fibre sizings, demonstrating improved fibre-matrix interfacial properties. Average mode I fracture toughness was also measured to be 10-30% higher than with the standard fibre sizing. Scanning electron microscopy and 3D depth composition were used to investigate fracture surfaces and determine the surface roughness. The novel reactive fibre sizing resulted in improved fibre-matrix adhesion and improved fracture toughness.

Abbreviations:

3D, three-dimensional; AFM, atomic force microscopy; APA-6, anionic polyamide 6; DCB, double cantilever beam; DMA, dynamic mechanical analysis; DSC, differential scanning calorimetry; GF/PA-6, glass-fibre/polyamide-6; LCM, liquid composite moulding; MW, molecular weight; NCF, non-crimp fabric; PA-6, polyamide 6; SEM, scanning electron microscopy; TGA, thermogravimetric analysis; TP-RTM, thermoplastic resin transfer moulding.

Keywords: A. Glass fibres, B. Interface/interphase, B. Fibre/matrix bond, B. Mechanical properties, Thermoplastic resin transfer moulding (TP-RTM).

1. Introduction

Thermoplastic polymers possess many desirable properties compared to their thermoset counterparts which make them suitable for high performance engineering applications. Their high molecular weight (MW) leads to better impact properties and improved resistance to fracture, with the additional benefits of weldability and recyclability. Despite their widespread use in the plastics industry, the use of thermoplastics in fibre reinforced composites has been limited, mainly due to their high melt viscosities which make the materials difficult to process, especially for liquid composite moulding (LCM) [1]. Low viscosity resins are preferred in order to fill and wet out reinforcements with high fibre volume fractions, so that high processing pressures are not required. The back pressures generated in LCM of thermoplastic polymers generally require large heavy-duty moulds and injection systems, and often present challenges such as dislodging of fibres in the mould cavity [2]. For these reasons, thermosets are the primary choice of matrix material used in such processes, and in order to use thermoplastics, other expensive intermediate processes are often required [3,4].

An additional disadvantage of using thermoplastics is the large difference between their glass transition temperature and the temperatures at which they are processed, compared to thermosets. This results in a high degree of shrinkage in parts, and hence, large residual stresses. The higher temperature requirements also mean greater energy usage, and often require longer cycle times due to heating and cooling.

Due to advancements in chemistry, furthered by a significant volume of research, a number of thermoplastic pre-polymer systems with low viscosities can be used in LCM processes [5–15]. These systems usually involve injecting a monomer and reactants, with a significantly lower viscosity compared to the polymerised melt, into a mould cavity containing a reinforcement material and allowing polymerisation to occur in-situ. This reactive moulding process, known as thermoplastic resin transfer moulding (TP-RTM), allows thermoplastic composite parts to be produced in a manner similar to traditional methods used for processing thermoset composites, avoiding the need for expensive heavy-duty equipment. One such system which has garnered attention in recent years is polyamide 6 produced by anionic polymerisation (APA-6) [5,16,17]. Here, the caprolactam monomer is mixed with an activator and catalyst, and injected into a fibre reinforcement contained within a mould. The added benefit of using this process is that the temperature required for polymerisation is ~130-180 °C, which is much lower than the melt temperature of polyamide 6 (220 °C), and the time for polymerisation is less than most thermosets [18]. Murray et al. developed two different (but similar) TP-RTM systems to produce APA-6 composites using both glass-fibres [19,20] and carbon-fibres [21] as a reinforcement.

Interfacial properties between the fibre and matrix can strongly influence composite mechanical properties, particularly those in the transverse direction for unidirectional laminates [22]. Previous research has focused on comparing the interfacial properties of APA-6 composites using different fibre sizings [23]; however, due to large void contents (up to 10% by volume) and low repeatability of the vacuum infusion process used, significant differences in interlaminar shear strength values were not shown. Johns Manville (CO, USA) have developed glass fibres with a reactive sizing that results in superior interfacial strength between the fibre and matrix, when used to reinforce APA-6. The glass fibre surface is coated with a sizing containing the activating group which causes PA-6 chain growth from the fibre surface, creating a strong interfacial bond [24]. The reactive sizing technology combined with the low viscosity precursor should theoretically result in enhanced mechanical properties, and initial testing has shown indications of this [25].

3

This study uses complementary techniques to investigate the reactive sizing developed by Johns Manville (US Patent No. US10954349 [26]), and to understand how it affects transverse composite properties. For comparison, throughout this study, the same fibres but with a standard silane agent are also used as a control. Scanning electron microscopy (SEM) and atomic force microscopy (AFM) were utilised to observe the distribution of sizing at both the micro- and nano-scale, respectively. In some cases, the sizing was removed and the unsized fibres were studied for comparison. Furthermore, thermogravimetric analysis (TGA) was used to determine the relationship between mass loss and temperature. In order to more accurately determine the amount of sizing on the fibres, larger quantity batches were used and mass loss was determined by both burn-off and reflux extraction.

Composite laminates were then manufactured from both sizing types. Quality assurance measures were put in place to compare the two sets of laminates in terms of voids, overall fibre volume fraction and local fibre packing density. It was important to fix the above variables so that any difference between the two cases could be almost exclusively attributed to the sizing effect. Transverse mechanical tests were carried out for each composite case and results were compared in terms of strength, stiffness and strain-to-failure. Double cantilever beam (DCB) tests were conducted to determine the mode I fracture toughness (G_{1c}) of each case. SEM images of the fractured surfaces were captured and the surface roughness across these surfaces was measured.

2. Methodology

2.1 Composite manufacture

2.1.1 Materials and storage

The polyamide matrix was produced from the following three raw materials: ε-caprolactam monomer, hexamethylene-1,6-dicarbamoylcaprolactam activator/caprolactam blend (BRUGGOLEN® C20p) and sodium-caprolactamate/caprolactam blend (BRUGGOLEN® C10), all provided by Brüggemann GmbH & Co. KG (Heilbronn, Germany). Due to the hydrophilic nature of the precursor materials and sensitivity of the polymerisation to moisture, special care was given to them in storage, preparation and processing. The materials were stored in air-tight bags within a sealed storage drum with desiccant, and a nitrogen purge was used before sealing the drum each time. During preparation, the materials were weighed and consequently exposed to air for a short period before being stored in jars with silica gel bags.

A 640 g·m^{-2} unidirectional non-crimp fabric (NCF) consisting of E-glass fibre rovings with a filament diameter of ~17 μm was used as the reinforcement material. The NCF consisted of polyester stitching perpendicular to the fibre direction in 5 mm increments. Two different Johns Manville rovings were used in the NCF: StarRov® 871, sized with a standard silane agent; and StarRov® 886 RXN, sized with a proprietary formulation by Johns Manville [26]. The StarRov® 886 RXN sizing consists of a *"coupling-activator compound with the formula S—X-(A)$_n$, where S represents a silicon-containing coupling moiety capable of bonding to the surface of glass fibres, X represents a linking moiety and (A)$_n$ represents one or more polymerisation activator moieties"*. This StarRov® 886 RXN sizing promotes covalent bonding between the fibres and polymer matrix due to initiation and chain growth from the activator moieties in the sizing. This enhances interfacial properties and as a result, the composite properties should be improved.

2.1.2 Manufacture

Composite laminates for extraction of tensile and flexural samples were manufactured using both the StarRov® 886 RXN and StarRov® 871-based fabrics. The procedures used were identical to those by Murray et al. [19] using the TP-RTM setup shown in Fig. 1.

The same injection and vacuum pressures were used for both cases. The samples for the DCB tests were extracted from laminates manufactured using the same TP-RTM machine and mould but using a 4 mm cavity

instead of the 2 mm used by Murray et al. [19]. These laminates consisted of 8 plies for each case. A non-adhesive insert was placed at the mid-plane through the thickness to act as a delamination initiator. The insert material used was a Teflon PFA film supplied by Lohmann Technologies (Milton Keynes, UK) with a thickness of 12.7 µm.

All mould surfaces were cleaned with acetone and then, two coats of Loctite Frekote 55NC mould release agent from Henkel (Düsseldorf, Germany) were applied. All taps and tubing used to transport the resin were cleaned with hot water at 90 °C to dissolve any residual caprolactam, followed by drying at 110 °C in air. For composite manufacturing, 350 mm x 390 mm plies of glass fibre NCF were cut and placed in the mould with the fibres aligned in the bulk flow direction. The mould surfaces were sealed using silicone rubber. A 4 mm cavity was used for making pure polymer and DCB Specimens, and a 2 mm cavity was used for the remainder of the composites. The mould was placed between the platens of the press, which were heated to 130 °C and a vacuum was drawn such that the cavity acted as a vacuum chamber to dry the fibre for at least 90 mins for each run.

2.1.3 Sample preparation

Due to their simple rectangular geometry, all composite samples were cut using a diamond blade cutting saw with coolant at a feed rate of ~300 mm·min^{-1} with the exception of differential scanning calorimetry (DSC) samples, which were cut using a Stanley knife blade. DCB specimens were prepared in accordance with ASTM D5528 – 13 using bored loading blocks to apply the opening force. Each sample (~3.8 mm x 25 mm x 170 mm) was cut such that the bore at the centre of the loading block (load line) would be 50 mm from the insert tip (crack initiation site) as shown in Fig. 2. The blocks were 25 mm x 25 mm x 15 mm, made from stainless steel and bored in the centre with a 6.1 mm diameter hole for a 6.0 mm pin. The bonding surfaces of the blocks and specimens were sanded using rough grit size sandpaper and cleaned with acetone prior to adhesion to the specimens. Polyolefin primer (Loctite 770) was applied to the surfaces, followed by bonding using a cyanoacrylate adhesive (Loctite 406). All samples were then dried under vacuum for 24 h at 50 °C and stored in either sealed polybags or Tupperware with desiccant until testing.

2.2 Fibre and sizing analysis

2.2.1　TGA

TGA was completed using a Mettler Toledo TGA/DSC1 (Columbus, USA). The experiments were

performed in air and nitrogen using approximately 30 mg of fibres cut into 5 mm long

pieces. The temperature cycle used a constant ramp rate of 10 °C·min^{-1} from 30 to 600 °C. Thereby, the mass

of the sizing (and any other agents) present on the glass was found.

2.2.2　Mass loss by burn-off

Approximately 10 g of conditioned fibres for each fibre type were subject to burn-off in a furnace with a

temperature ramp of 10 °C·min^{-1} from 30 to 600 °C, followed by an isotherm at 600 °C for 30 mins.

Following this, the samples were cooled to 110 °C, after which the new mass was recorded. This ensured the

specimens did not have enough time to absorb moisture at any point prior to weighing. An OHAUS AX324

analytical balance (New Jersey, USA) was used to record masses and a Nabertherm L15/11 Muffle Furnace

(Lilienthal, Germany) was used to complete the burn-off.

2.2.3　Condensation reflux extraction

SEM and AFM were carried out on glass fibres with the two different sizings (871 and 886), as well as on

unsized fibres to allow for a more robust comparison. The unsized fibres were prepared by dissolving the

sizing from the fibre surface using condensation reflux extraction. The apparatus for extraction consisted of a

round-bottom boiling flask and a DWK Quickfit condenser coil. Approximately 10 g of fibre cut into 50 mm

long tows was added to the flask for each batch. Acetone (250 mL) was used as the solvent and water as the

cooling medium in the condenser. The boiling flask was heated using an Electrothermal EMA0100/CEB

(Stone, UK) heating mantle such that the solvent was brought to a vigorous boil and the reflux was run for 24

h. As well as being used for preparing unsized samples for microscopy, this method was also used to

measure the mass of the sizing on fibres. In doing so, the fibres were dried and weighed using an analytical

balance both before and after extraction to determine the mass loss which was attributed to the sizing.

2.2.4   SEM characterisation

For both of the fibre sizing cases, individual fibres were carefully removed from bundles using tweezers and cut to lengths of ~20 mm using scissors. The unsized fibres were prepared by burn-off using methods described in Section 2.2.2. The stage for the SEM was removed and cleaned with acetone before use. A number of fibre samples for each case were placed on the SEM stage in separate batches. The stage was placed in the Hitachi TM4000Plus SEM (Tokyo, Japan) and the samples were viewed at magnifications of 4,000x using an accelerating voltage of 2 kV.

2.2.5   AFM characterisation

AFM was utilised to image the surface of each fibre case at the nanoscale. All imaging was performed in tapping mode using a Bruker-JPK Nanowizard 4 (Bruker, Nano GmbH, Berlin, Germany) in air at ambient conditions. Bruker RTESPA cantilevers with a spring constant of 40 N/m and a nominal tip radius of 2 nm were used for all imaging. As the fibres had relatively small diameters, the scan size for each image was 1 μm x 1 μm. Height and 3D images were obtained for the three fibre types. Furthermore, profile plots were obtained from the height images which showed the surface topography of each fibre in greater detail. The average arithmetic surface roughness (Ra) was calculated from at least four separate images for each fibre type. The profile plots and surface roughness values were obtained after the AFM images had undergone flattening in order to eliminate any influence from the fibre curvature.

2.3 Composite testing

2.3.1   Composite quality assessment

The quality assurance techniques described by Murray et al. [19] were used to measure thickness, density, fibre volume and void volume fraction/distribution. The thickness variation was measured using a Kroeplin Digital C450 electronic measuring gauge at 25 locations evenly distributed in a 5 × 5 pattern across each laminate. Density values were determined from 15 mm × 15 mm samples taken from 9 locations evenly distributed across each laminate. The mass of each sample was measured in both air and water using an OHAUS AX324 analytical balance and a density determination kit. Archimedes' principle was then used to determine the density in accordance with ISO 1183-1:2019 Method A. To determine the fibre volume

fraction (V_f) of composite samples, the same 9 samples used for density measurements were used for burn off in accordance with ISO 7822:1999 Method A.

Due to the effects of fibre packing density in bundles, it was essential to make sure that the staggering of bundles in both cases was similar before comparing transverse properties. Longitudinal tensile tests were carried out on both composite cases as an additional technique to demonstrate similar quality between the two cases prior to studying interfacial properties. These tests were carried out in accordance with BS EN ISO 527-5:2012, using 250 mm × 15 mm × 2 mm samples. The samples were end-tabbed and tested on an MTS C45.305 machine using a 300 kN load cell, using a crosshead speed of 2 mm/min. Strain values were measured by painting a speckled pattern on samples prior to testing, and tracking dimensional changes using an IMETRUM AVX video gauge. Due to small differences in fibre volume fractions, all longitudinal tensile results were normalised to a fibre volume fraction of 50%.

2.3.2   Polymer matrix characterisation

The polymer quality was characterised by measuring the degree of conversion, degree of crystallinity, melt temperature and glass transition temperature (T_g). The first three properties were determined using reflux extraction and DSC techniques described by Murray et al. [19], while T_g was determined by dynamic mechanical analysis (DMA). It should be noted that the technique used to measure the degree of conversion doesn't account for oligomers or low MW polymer which are also extracted. While the strict definition of conversion includes these, the measurement accounts for high MW polymer only. The T_g was determined using DMA. A three-point bending configuration was used in accordance with ISO 6721-11:2012 on a Triton 2000 DMA (Mansfield, USA). Three 10 mm x 35 mm samples from each plate were tested using a 30 mm span with a displacement of 0.05 mm. The samples were dried under vacuum for 24 h at 50 °C prior to testing. The tests were run at a frequency of 10 Hz from room temperature up to 180 °C at a ramp rate of 5 °C·min^{-1}. The T_g was determined using both the peak in loss modulus and tan δ.

2.3.3   Transverse properties

Transverse testing gives a more holistic view of the sizing performance by taking the aforementioned practical considerations into account, such as fibre packing density and voids due to stitching, which are not captured by single fibre-matrix tests. Transverse testing was carried out for both cases in tension and flexure.

Tensile tests were carried out in accordance with BS EN ISO 527-5:2012 using Type B specimens (250 mm × 25 mm × 2 mm) on an Instron 3369 screw-driven machine with a 10 kN load cell. A crosshead speed of 1 mm/min was used and the IMETRUM AVX video gauge was used to measure strain.

2.3.4   DCB testing

While fracture toughness is something of interest in general for the GF/APA-6 material, the DCB test can also be used as a method for measuring the strength of the interface. The tests were carried out in accordance with ASTM D5528 − 13 on an Instron 3369 (Norwood, USA) using a 1 kN load cell. The specimens used in these tests were fully consolidated at one end but split in two halves at the other end, separated during manufacture by a thin insert as described in Section 2.1.2. To track the crack length during testing, the IMETRUM AVX video gauge was used. For further details of the testing method used, see the supplementary material.

2.3.5   Surface Roughness

Surface roughness measurements of fracture surfaces of tested DCB specimens were taken using a Keyence VHX 7000 digital microscope (Osaka, Japan) by taking multiple images and stitching them together. Multi-focus image fusion (or 3D depth composition) was used to obtain optimum focus at different depths and a 3D image was generated. Imaging was carried out over a focused area of 4 bundles (shown in Fig. 3 (a)) at high magnifications and was carried out over the entire sample width (shown in Fig. 3 (b)) at lower magnifications. Surface plots were generated at various cross sections across specimens at both magnifications (shown in Fig. 3 (c)-(d)), both in the tested crack area and in the area where the insert was placed. The surface roughness was plotted over a width of 3 bundles from crest-to-crest with the "zero height" datum positioned at the average height for each case. The Ra and the root mean square roughness (Rq) were measured for each fibre type.

3. Results and Discussion

3.1 Fibre and sizing results

3.1.1 Mass loss

The TGA results (Fig. 4) demonstrate that there is no volatile mass loss in the water vaporisation region (~100 °C) which indicates that the specimens were appropriately conditioned prior to the experiment. In this case, the measured change in mass can be attributed to the mass of the sizing.

The mass loss over time from TGA can be observed in Fig. 4, in which the primary area of interest is between 130 and 200 °C as this is the temperature range where polymerisation occurs. Initially, both fibre types lose very little mass in both air and nitrogen; however, the rate of loss in the 886 and 871 fibres in air increases above ~178 °C and ~190 °C, respectively. If the exotherm in the mould causes temperatures to rise to this degree, there is a possibility that the sizing may become damaged. If this is the case, it would reduce the sizing's effectiveness in increasing the interfacial strength. The mass loss for both cases was observed to be marginally smaller in the nitrogen environment, which suggests there is minor oxidation occurring in both cases in air. The conditions in nitrogen would be similar to the conditions in the mould cavity under vacuum during processing, as oxidation cannot occur.

The total mass loss after TGA, burn-off and reflux extraction are given in Table 1. All techniques showed that the amount of sizing on 886 fibres by mass was less than that on the 871 fibres by 9-22%. The mass loss using burn-off was noticeably greater than that using reflux extraction. It is possible that acetone did not dissolve the sizings completely. The sizing makes up ~0.5% of the total weight of fibres. This is slightly more than the 0.3% value stated for each in the Johns Manville data sheets.

3.1.2 SEM imaging

Representative SEM images of the 871, 886 and unsized fibres are shown in Fig. 5. Differences in topography of the sizings can be observed from the three images. Fig. 5 (a) clearly demonstrates that the distribution of sizing on the 871 is relatively rough, whereas that for the 886 shown in Fig. 5 (b) is even and generally very smooth, though there were signs of agglomerates of sizing in certain locations. As expected, the unsized fibres also appear to be very smooth. The diameter of fibres (and sizing) was measured from 12

samples for each case and had values of 16.62 ± 1.12, 16.15 ± 1.26 and 16.14 ± 1.29 μm for the 871, 886 and

unsized fibres, respectively. While the average diameter value for the 871 was greater than that for the 886,

indicative of greater amounts of sizing, the difference was not statistically significant with a p-value of 0.34.

3.1.3   AFM imaging

Fig. 6 presents typical AFM height images for each fibre type with corresponding cross-sectional profile

plots which show the surface of the fibres in greater detail. Corresponding 3D images (not flattened) are also

presented which clearly show the surface topography of the sizing on the curved fibres. The method of fibre

imaging and analysis followed work of Mamalis et al. [27][28]. As with the SEM imaging, the results

demonstrated that the topography of the sizing is very different on each fibre type. On the unsized fibres

(Fig. 6 (a) – (c)), the topography is mostly smooth with only a few discernible features which are likely small

remnants of original sizing. Despite this, the unsized fibres were still extremely smooth with an average

surface roughness of 0.8 nm, presenting a valid control. The sizing on the 871 fibres (Fig. 6 (d) – (f)) formed

a distinct dendritic structure with a height that generally ranged from 5 – 15 nm. The dendritic structure was

very homogeneous across large areas of the fibre surface (see supplementary material) and the average

surface roughness of the 871 fibres was 3.5 nm. In contrast, the sizing on the 886 fibres (Fig. 6 (g) – (i)) had

a very different surface topography. The surface was generally smooth but contained fairly large,

sporadically located aggregates across the surface. This is clearly observed in the 3D image (Fig. 6 (i)) which

shows a few large aggregates located on an otherwise smooth fibre surface. Consequently, the average

surface roughness of the 886 fibres was 2.7 nm. The AFM results suggests that the nature of the 886 sizing

and 871 sizing are very different on the fibres and observations of the general distribution of sizing matches

with those seen using SEM. The 871 sizing has a very distinct topographical structure whereas the 886 sizing

forms sporadically positioned and irregularly-shaped aggregates with larger heights. AFM phase images

(images in supplementary material) qualitatively demonstrated that the viscoelastic properties across each

fibre surface were mostly homogeneous [29].

3.2 Composite testing

3.2.1 Composite quality assessment

Normalised mechanical test results for composites manufactured using the 871 and 886 fabrics are summarised in Table 2. Firstly, the 871 composites are on average 3.75% thicker than the 886 composites. This was noticed in almost all manufactured composites and was attributed to the sizing on the 886 fibres, which allowed slightly more preform compression during processing. As expected, the longitudinal modulus is the same for both; however, the reduced longitudinal strength in the 886 composites may be due to greater load transfer between the fibres and matrix as a result of the reactive sizing.

SEM images from the composite cross sections are presented in Fig. 7. It is clear from Fig. 7 (a) and (b) that the staggering of the bundles for both the 886 and 871 fibres is almost identical. The reason for the less densely packed bundles in the upper plies of the 871 case is due to their distance from the next stitch. There is only an indication of very minor macro voids in each case, which occurs at the stitching, while Fig. 7 (c) and (d) show that the wet-out of bundles is excellent with no indication of any significant micro voids in either. Fig. 7 (e) and (f) show the fibres in the transverse direction. Fig. 7 (e) indicates macro voids in the 886 composites but only at the stitch. The reason this is observed in the 886 but not in the 871 is due to the depth (into the page) that the sample were cut/polished. The former shot has been taken at a section that is close to resin rich trenches for most of the bundles, as described by Murray et al. [19]. This is indicated by the relatively low fibre volume fraction in the image compared to the equivalent for the 871 fibre case. It should be noted that while average fibre volume fractions are in the 51-54% region, locally in bundles it is closer to 65%. The effects of this on mechanical performance is described in-depth by Murray et al. [19].

3.2.2 Polymer matrix characterisation

The results for degree of conversion, degree of crystallinity, melt temperature and T_g are presented in Table 3. The average value of conversion to high MW polymer for the 886 is 2% less than that for the 871 material. This reduction is possibly due to the reactive sizing which acts as an initiation site for chain growth. The effects of the fibre surface sizing on the matrix properties would be similar to adding additional initiator to the system; however, these effects would only apply to the polymer at the fibre surface, creating a sort of interphase with chains growing radially from the fibre surface. By definition, the initiation process involves

the formation of oligomers. Due to an increased density of chains competing for growth from the surface of the 886 sizing, it is more likely that termination would occur prematurely in these regions due to local monomer depletion. As a result, the overall degree of conversion to high MW polymer may be restricted [30]. Due to the larger number of chains with an unchanged amount of monomer available during polymerisation, the average chain length is shortened, reducing the average MW. The average T_g is only slightly higher for the 886 case (i.e., barely significant statistically). Even though lower MW is generally associated with a lower T_g in accordance with the Flory-Fox relationship [31], the increased restriction in chain mobility (due to more chains in the 886 case) may counteract this with an upward shift in the temperature required for mobilisation. Typical DSC curves for both cases are shown in Fig. 8. The degree of crystallinity for both cases is similar, and considering the large error (due to numerous dependencies) in the method to calculate values, drawing any further conclusions from these results would be difficult. Overall, no significant differences were identified between the matrices in the 886 and 871 composites.

3.2.3   Transverse properties

Results from transverse tensile and flexural tests are presented in Table 4 and Fig. 9 in terms of strength, modulus and strain at maximum stress. Properties for the pure matrix and a commercial GF/PA-6 organosheet with a similar fibre volume fraction are included to contextualise results [19,32]. Welch's t-test [33] was used to determine statistical significance ($p < 0.05$) between the 871 and 886 cases for each test metric, and values which demonstrate statistical significance are shaded in Table 4. The flexural strength and modulus were notably higher (20% higher average strength, 28% higher average modulus) for the 886 case with significant statistical differences ($p = 0.02$ and 0.00, respectively). The average transverse tensile strength of the 886 composite was 12% higher than that of the 871 composite. While the difference in modulus between the two was practically negligible ($p = 0.92$), the increased strength and strain-to-failure indicate that the reactive sizing may have enhanced mechanical performance, with p-values of 0.11 and 0.09, respectively. Fig. 12 (a) and (c) show SEM images of representative transverse tensile fracture surfaces for the two cases. Overall, the results indicate that their appearance is generally similar to one another. Fibre tracks are more visible in the 871 case, however, which indicates cleaner pull-out and hence adhesive failure. Futhermore, the agglomerations of ductile matrix drawn from around the fibre surface are smaller for the 886 but have more splinters, possibly indicating more local sites with superior bonding.

3.2.4   Fracture toughness

Representative plots for load-extension, load-delamination growth and G_1-delamination growth are presented in Fig. 10. Values for $G_{1C\,VIS}$, $G_{1C\,Max}$ and $G_{1C\,Avg}$ were calculated from DCB test data for both the 871 and 886 cases and are given in Table 5. In terms of the average G_{1C} across sample sets, the 886 outperforms the 871 using all three metrics of determination by 29%, 14% and 10%, respectively. It should be noted that despite indications of differences in terms of G_{1C} between the 871 and 886 cases, the statistical significance of the difference is weak ($p = 0.33$, 0.21 and 0.26, respectively). Fibre bridging occurred in samples, but only in the immediate area up to approximately 10 mm behind the crack as it grew. This, combined with plastic deformation along the cracked region may explain the reason for such large differences between initiation values determined visually and at maximum load.

Due to the large linear deflections observed in Fig. 10 (a), it would be fair to question if plastic deformation occurred in the sample itself in the split ends (cantilevers). After unloading of the specimens, these ends did not fully close to their original position, indicating a degree of plastic deformation. The test standard, however, states that small amounts of plastic deformation are acceptable. Thicker specimens with an increased number of plies may have been more suitable for this test type as they would have been stiffer. The large deflections resulting from the low stiffness made it necessary to apply correction factors (F and N), as discussed in the supplementary material, which added to the complexity of the test. More importantly, thicker specimens would have resulted in lower flexural stresses, hence less plastic deformation within the cantilevers.

Ductile fibrillation in the SEM images of fractured surfaces in Fig 11 (b) and (d) indicates that significant plastic deformation occurred for both cases at the fibre-matrix interface. The images show a high degree of adhesive failure in both cases but with cleaner pull-out of fibres in the 871 case, leaving a smoother surface. The nature of the matrix in each case is different. The matrix in the 886 case has a more fibrous appearance as was seen in the SEM images of the transversely tested samples. It is likely that, due to the higher strength of the interfacial bonding in the 886 samples (shown in Table 4), the material experiences higher strains to failure before finally failing at the interface.

The surface plots and roughness values for both cases are presented within Fig. 12 and Table 6, respectively. As a reference, roughness measurements of the area separated by the insert were also measured. The Ra and

Rq values in the cracked region for the 886 case are higher than those for the 871. The jagged peaks and crests on the 886 cracked surface plot indicate that large amounts of plastic deformation occurred prior to separation of the surfaces. This may be due to fibre bridging or higher strain in the matrix, however, both would indicate a superior bond at the interface. This reinforces the aforementioned explanation as to why the 886 cracked surface appears to be more fibrous. High strength and strain both contribute towards the calculation of G_{1C} by increasing the force and displacement terms in the equation, and so, it is unsurprising that the values for the 886 case are greater than those for the 871.

3.3 Overall Discussion

The average diameter of the 871 fibres (including sizing) was greater than the 886, indicating a larger volume of sizing on the former. This was confirmed by TGA and burn-off studies. Both SEM and AFM showed that the distribution of sizing across the 886 fibres was more sporadic compared to the 871 fibres. Surface roughness (Ra) measurements of the 871 fibres were ~30 % higher than the 886. At a smaller scale, the 871 sizing is more ordered, forming clear dendritic structures, whereas the 886 sizing shows no signs of order at the same level of magnification.

Mechanical testing in the transverse direction proved that there was a marked increase in flexural strength and modulus, and tensile strength in the 886 composites compared to the 871 composites. This was attributed to superior fibre-matrix interfacial adhesion in the 886 composites due to the reactive sizing. The average mode I fracture toughness value for the 886 material was higher than the 871 by 10-30%, depending on which metric was used for its determination. Welch's t-test method showed that there was no statistical significance between the two cases which was unsurprising considering the large scatter in test results. Some factors which likely contributed to this scatter include variations in specimen dimensions as well as variations in the large number of variables involved in calculating G_{1C} values. The fracture toughness for both cases is significantly higher than most thermoset composites and competes well with PEEK composites [34–36]. Surface roughness measurements showed that there was much greater distortion in the cracked region of the 886 material compared to that of the 871. This is thought to be due to the larger strains to failure, allowed by the greater interfacial strength.

Additional SEM images were taken of the 886 composite fracture surface after longitudinal flexural testing, and are given in the supplementary material. These images expose the difference between the 886 and 871

composites more clearly than those for the transverse fracture surfaces. In the SEM for the 886 case, the fibres are barely visible, meaning that cohesive failure occurred, indicating that the fibre-matrix interface is relatively strong. This is very different to the relatively bare fibres for the fractured 871 case. These images also show ductile drawing of the matrix from the fibre surface for the 886 case. The matrix seems to have undergone a lot of plastic deformation but still remains bonded to the fibre surface, which is further evidence that the interface is sufficiently strong.

It should be noted that attempts were made to carry out single-fibre pull-out tests; however, due to unsatisfactory samples preparation, mainly due to the complexity of polymerisation with individual fibres, large scatter resulted. For this reason, the results were inconclusive, and have therefore been placed in the supplementary material to this paper.

Overall, there are indications that the 886 sizing results in greater composite strength and fracture toughness compared to the 871 sizing; however, with limited statistical significance for some of the test results. For greater certainty, some of these tests would need to be repeated with larger specimen batches. The samples would need to be manufactured with perfectly staggered plies and a prudent humidity/temperature conditioning regime would be required before testing. Considering the attention given to quality assurance in trying to fix as many variables as possible in this (other than those being investigated), it is believed that this study provides a detailed contribution to the overall investigation.

4. Conclusions

Glass-fibres with two different sizings, one with a reactive agent and one with a standard silane agent, were compared in terms of their form, geometry and mass. The fibres (in the form of a fabric) were incorporated as a reinforcement material into polyamide-6 composites, produced using TP-RTM, and their mechanical properties were determined to measure the effects of the sizings.

Research indicates that oxidation occurs in the reactive sizing (886) at lower temperatures (c. 178 °C) than that for the silane sizing (c. 190 °C). If the temperature of the sizing is at or above these values for any significant period of time, the sizing will start to experience some degradation, which would likely diminish its benefits in terms of interfacial adhesion. The distribution of sizing on the fibre surface for the reactive

case was less consistent than that for the silane case. The same was shown on the nano-scale where the structure for the latter was shown to be dendritic, while that of the former was more heterogeneous.

Mechanical testing of composites manufactured using both fibre types proved with a high degree of statistical significance that composites with the reactive sizing outperformed those with the silane sizing in terms of average transverse flexural strength and modulus (by 20% and 28%, respectively). The average transverse tensile strength of the composite with the reactive sizing was superior to that with the silane sizing (by 12%), albeit with more limited statistical significance. DCB testing showed that on average, the mode I fracture toughness for the composite with the reactive sizing was higher than that with the silane sizing (by 10-29%) but once again, with limited statistical significance. The surface roughness of the former was higher in the cracked region and more sporadic after testing. This corresponds to the microscopy results and indicates that although the distribution of sizing is not uniform in the reactive case, the bonding where present, is significant. Overall, it was demonstrated that the APA-6 composites had superior toughness to those using most thermoset matrices. The reactive sizing resulted in improved fibre-matrix adhesion and improved fracture toughness, indicating that its use in structural applications can result in a more durable structure with a higher resistance to fracture.

Data Availability

The raw/processed data required to reproduce these findings cannot be shared at this time due to technical or time limitations.

References

[1]   Chang IY, Lees JK. Recent Development in Thermoplastic Composites: A Review of Matrix Systems and Processing Methods. J Thermoplast Compos Mater 1988;1:277–96. https://doi.org/10.1177/089270578800100305.

[2]   Tempelman E, Shercliff H, Ninaber van Eyben B. Resin transfer molding. Manuf. Des., 2014, p. 171–86. https://doi.org/10.1016/B978-0-08-099922-7.00010-X.

[3]   Ye L, Klinkmuller V, Friedrich K. Impregnation and Consolidation in Composites Made of GF/PP Powder Impregnated Bundles. J Thermoplast Compos Mater 1992;5:32–48. https://doi.org/10.1177/089270579200500103.

[4]   McDonnell P, McGarvey KP, Rochford L, Ó Brádaigh CM. Processing and mechanical properties evaluation of a commingled carbon-fibre/PA-12 composite. Compos - Part A Appl Sci Manuf 2001;32:925–32. https://doi.org/10.1016/S1359-835X(00)00155-X.

[5]   Ageyeva T, Sibikin I, Karger-Kocsis J. Polymers and related composites via anionic ring-opening polymerization of lactams: Recent developments and future trends. Polymers (Basel) 2018;10:357. https://doi.org/10.3390/polym10040357.

[6]   Šebenda J. Anionic Ring-opening Polymerization: Lactams. Compr. Polym. Sci. Suppl., 1989, p. 511–30. https://doi.org/10.1016/B978-0-08-096701-1.00097-5.

[7]   van Rijswijk K, Lindstedt S, Vlasveld DPN, Bersee HEN, Beukers a. Reactive processing of anionic polyamide-6 for application in fiber composites: A comparitive study with melt processed polyamides and nanocomposites. Polym Test 2006;25:873–87. https://doi.org/10.1016/j.polymertesting.2006.05.006.

[8]   Udipi K, Dave R, Kruse R, Stebbins L. Polyamides from lactams via anionic ring-opening polymerization: 1. Chemistry and some recent findings. Polymer (Guildf) 1997;38:927–38. https://doi.org/10.1016/S0032-3861(96)00566-6.

[9]   Russo S, Casazza E. 4.14 – Ring-Opening Polymerization of Cyclic Amides (Lactams). Polym. Sci. A Compr. Ref., 2012, p. 331–96. https://doi.org/10.1016/B978-0-444-53349-4.00109-6.

[10]   Davé RS, Kruse RL, Udipi K, Williams DE. Polyamides from lactams via anionic ring-opening polymerization: 2. Kinetics*. Polymer (Guildf) 1997;38:939–47. https://doi.org/10.1016/S0032-3861(96)00568-X.

[11]   Davé RS, Kruse RL, Udipi K, Williams DE. Polyamides from lactams via anionic ring-opening polymerization: 3. Rheology. Polymer (Guildf) 1997;38:949–54. https://doi.org/10.1016/S0032-3861(96)00568-X.

[12]   Šebenda JAN. Lactam Polymerization. J Macromol Sci Part A - Chem Pure Appl Chem 1972;A6:1145–99. https://doi.org/https://doi.org/10.1080/10601327208056889.

[13]   Obande W, Mamalis D, Ray D, Yang L, Ó Brádaigh CM. Mechanical and thermomechanical characterisation of vacuum-infused thermoplastic- and thermoset-based composites. Mater Des 2019;175:107828. https://doi.org/10.1016/j.matdes.2019.107828.

[14]   Obande W, Gruszka W, Garden JA, Wurzer C, Ó Brádaigh CM, Ray D. Enhancing the solvent

resistance and thermomechanical properties of thermoplastic acrylic polymers and composites via reactive hybridisation. Mater Des 2021;206:109804. https://doi.org/10.1016/j.matdes.2021.109804.

[15]   Qin Y, Summerscales J, Graham-Jones J, Meng M, Pemberton R. Monomer selection for in situ polymerization infusion manufacture of natural-fiber reinforced thermoplastic-matrix marine composites. Polymers (Basel) 2020;12:1–25. https://doi.org/10.3390/polym12122928.

[16]   Semperger OV, Suplicz A. The effect of the parameters of t-rtm on the properties of polyamide 6 prepared by in situ polymerization. Materials (Basel) 2020;13:1–11. https://doi.org/10.3390/ma13010004.

[17]   Osváth Z, Szőke A, Pásztor S, Závoczki LB, Szarka G, Iván B. Recent Advances in the Synthesis and Analysis of Polyamide 6 and Products Therefrom : From Polymerization Chemistry of ε-Caprolactam to Thermoplastic Resin Transfer Molding (T-RTM) 2020;4. https://doi.org/10.19080/AJOP.2020.04.555629.

[18]   Hexcel Corporation. HexFlow ® RTM 6 datasheet 2018:1–4.

[19]   Murray JJ, Robert C, Gleich K, McCarthy ED, Ó Brádaigh CM. Manufacturing of unidirectional stitched glass fabric reinforced polyamide 6 by thermoplastic resin transfer moulding. Mater Des 2020;189:108512. https://doi.org/10.1016/j.matdes.2020.108512.

[20]   Murray JJ, Allen T, Bickerton S, Bajpai A, Gleich K, McCarthy ED, Ó Brádaigh CM. Thermoplastic RTM: Impact Properties of Anionically Polymerised Polyamide 6 Composites for Structural Automotive Parts. Energies 2021;14:5790. https://doi.org/10.3390/en14185790.

[21]   Murray JJ, Allen T, Bickerton S, Gleich K, McCarthy ED, Ó Brádaigh CM. Impact Performance of Thermoplastic Resin Transfer Moulded Carbon Fibre Composites. SAMPE Eur. Conf., Amsterdam: 2020, p. 3–12. https://doi.org/10.5281/zenodo.5117998.

[22]   Murray JJ, Pappa EJ, Mamalis D, Breathnach G, Doyle A, Flanagan T, Di Noi S, Ó Brádaigh CM. Characterisation of carbon fibre reinforced powder epoxy composites for wind energy blades. Proc. 18th Eur. Conf. Compos. Mater., Athens: 2018.

[23]   van Rijswijk K, van Geenen A, Bersee HEN. Textile fiber-reinforced anionic polyamide-6 composites. Part II: Investigation on interfacial bond formation by short beam shear test. Compos Part A Appl Sci Manuf 2009;40:1033–43. https://doi.org/10.1016/j.compositesa.2009.02.018.

[24]   Johns Manville. StarRov ® 886 Data Sheet 2021.

[25]   Zhang M, Yohannes A, Block M, Gleich K, Asrar J. THERMOPLASTIC COMPOSITES FROM REACTIVE RESIN SYSTEMS – CHALLENGES AND OPPORTUNITIES. 19Th Int. Conf. Compos. Mater., Montreal: 2013.

[26]   Johns Manville, Zhang M, Gleich KF, Yohannes A, Block MJ, Asrar J. Fiber Reinforced Composites Made with Coupling-Activator Treated Fibers and Activator Containing Reactive Resin.

US10954349, 2021.

[27] Mamalis D, Murray JJ, McClements J, Tsikritsis D, Koutsos V, McCarthy ED, Ó Brádaigh CM. Novel carbon-fibre powder-epoxy composites: Interface phenomena and interlaminar fracture behaviour. Compos Part B Eng 2019;174. https://doi.org/10.1016/j.compositesb.2019.107012.

[28] Mamalis D, Floreani C, Ó Brádaigh CM. Influence of hygrothermal ageing on the mechanical properties of unidirectional carbon fibre reinforced powder epoxy composites. Compos Part B Eng 2021:109281. https://doi.org/10.1016/J.COMPOSITESB.2021.109281.

[29] Lasseuguette E, McClements J, Koutsos V, Schäfer T, Ferrari MC. Ionic liquid mediated surface micropatterning of polymer blends. J Appl Polym Sci 2018;135:46109. https://doi.org/10.1002/app.46109.

[30] Ueda K, Hosoda M, Matsuda T, Tai K. Synthesis of High Molecular Weight Nylon 6 by Anionic Polymerization of ε-Caprolactam. Formation of Cyclic Oligomers. Polym J 1998;30:186–91. https://doi.org/https://doi.org/10.1295/polymj.29.568.

[31] Fox TG, Loshaek S. Influence of molecular weight and degree of crosslinking on the specific volume and glass temperature of polymers. J Polym Sci 1955;15:371–90. https://doi.org/10.1002/pol.1955.120158006.

[32] SGL Group. Unidirectional glass fiber tape with thermoplastic matrix datasheet 2017.

[33] Welch BL. The Generalization of `Student's' Problem when Several Different Population Variances are Involved. Biometrika 1947;34:28. https://doi.org/10.2307/2332510.

[34] Samborski S, Gliszczynski A, Rzeczkowski J, Wiacek N. Mode I interlaminar fracture of glass/epoxy unidirectional laminates. Part I: Experimental studies. Materials (Basel) 2019;36:1119–27. https://doi.org/10.3390/ma12101607.

[35] ASTM D5528-13: Standard test method for mode I interlaminar fracture toughness of unidirectional fiber-reinforced polymer matrix composites. 2014. https://doi.org/10.1520/D5528-13.2.

[36] Pappa EJ, Quinn JA, Murray JJ, Davidson JR, Ó Brádaigh CM, McCarthy ED. Experimental Study on the Interlaminar Fracture Properties of Carbon Fibre Reinforced Polymer Composites with a Single Embedded Toughened Film. Polymers (Basel) 2021;13:4103. https://doi.org/https://doi.org/10.3390/ polym13234103.

[37] Evonik Industrial. VESTAPE Uni-directional tapes for structural lightweight design datasheet n.d.

[38] Floreani C, Robert C, Alam P, Davies P, Brádaigh CMÓ. Mixed-Mode Interlaminar Fracture Toughness of Glass and Carbon Fibre Powder Epoxy Composites — For Design of Wind and Tidal Turbine Blades. Materials (Basel) 2021;14:2103. https://doi.org/https://doi.org/10.3390/ma14092103.

[39] Chen JH, Schulz E, Bohse J, Hinrichsen G. Effect of fibre content on the interlaminar fracture

toughness of unidirectional glass-fibre / polyamide composite. Compos Part A Appl Sci Manuf 1999;30:747–55. https://doi.org/https://doi.org/10.1016/S1359-835X(98)00188-2.
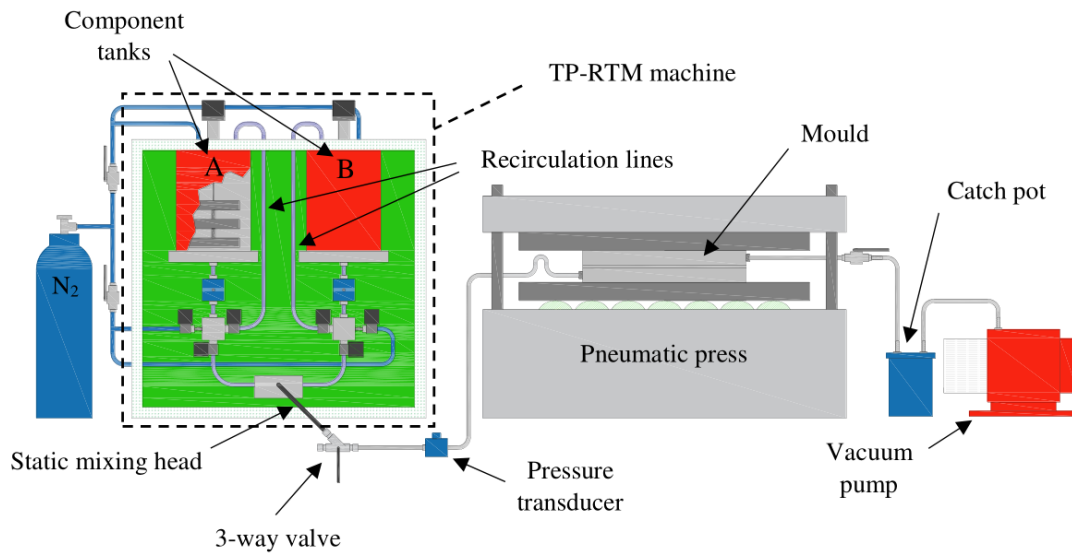
Figures

Fig. 1: Illustration of the assembled TP-RTM setup for polymer/composite manufacture [19].
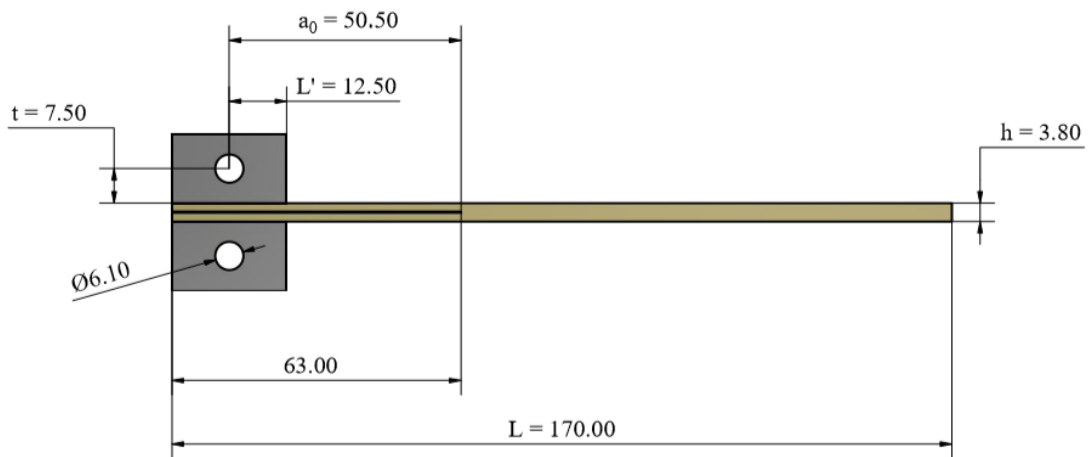

Fig. 2: Dimensions of the DCB specimens and loading blocks given in mm. Note that the width of specimens was 25 mm (into the page).
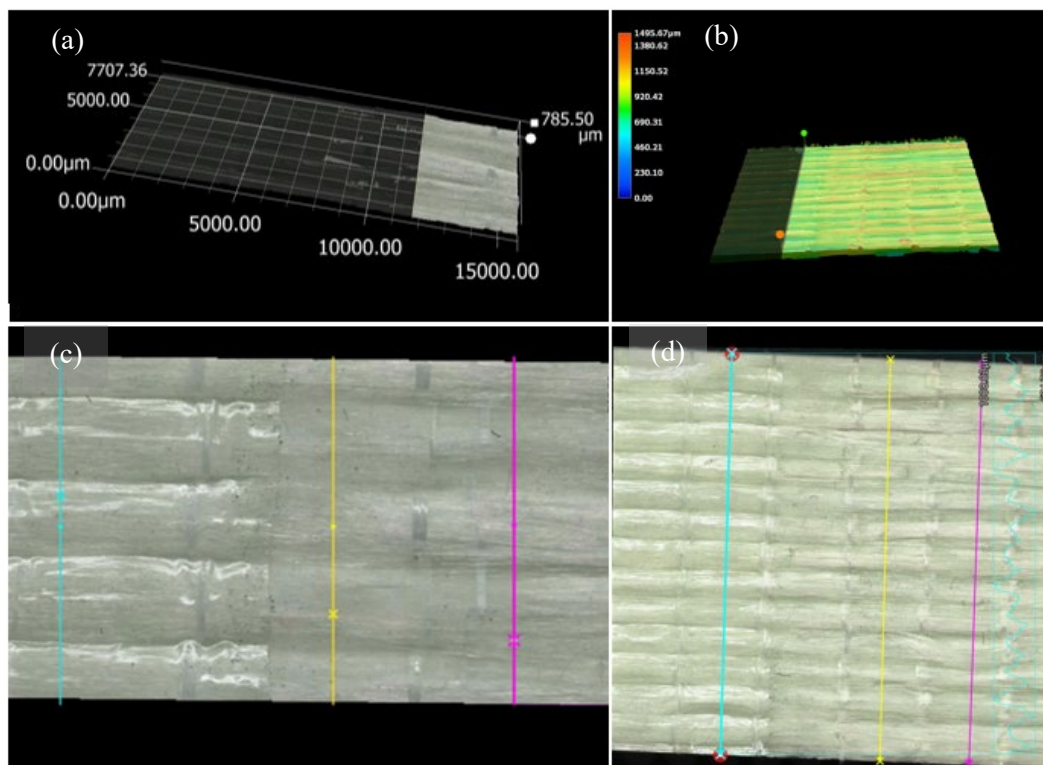
Fig. 3: Examples of 3D surface plots generated by multi-focus image fusion at (a) a high-magnification over four fibre bundles, at (b) a low-magnification over the entire sample width; and plan views demonstrating locations where cross sections were taken for surface roughness characterisation (represented by the coloured lines) at (c) a high-magnification and (d) a low-magnification.
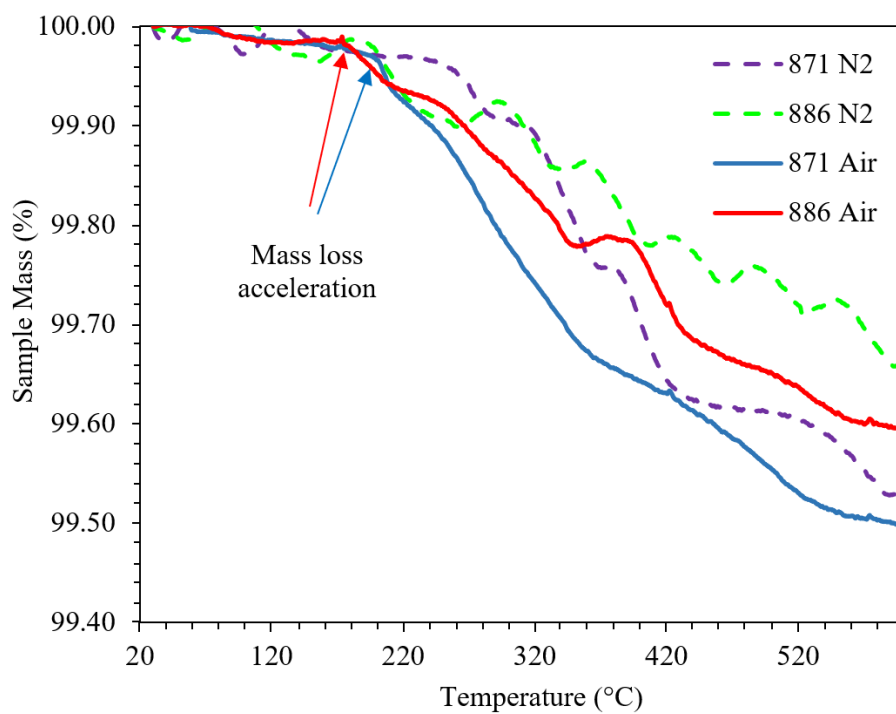

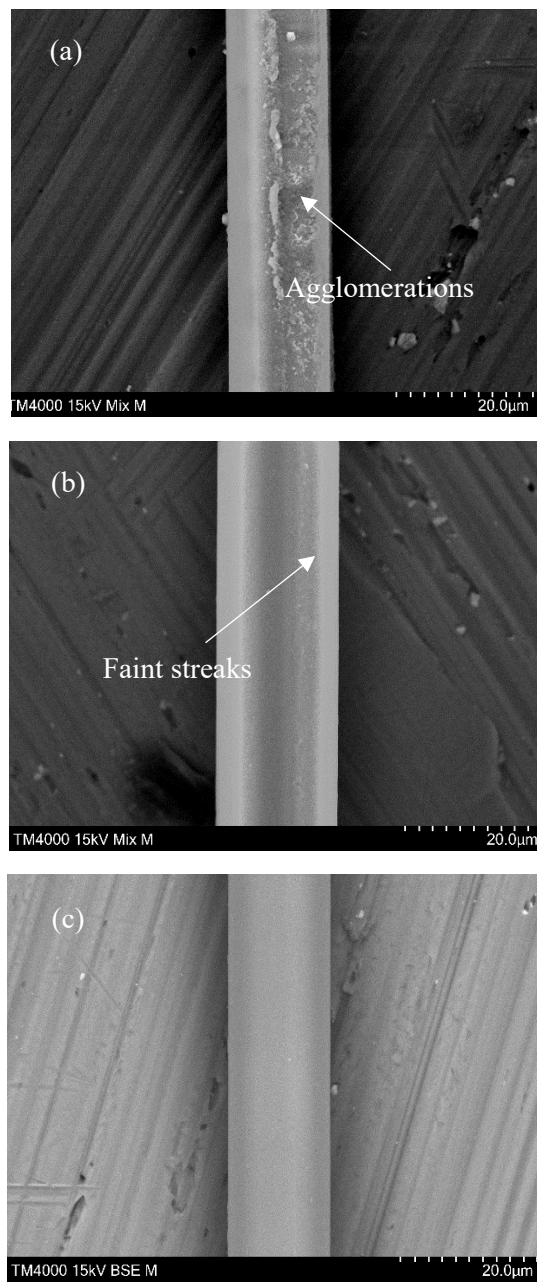**Fig. 4:** TGA curves for the 871 and 886 RXN sizings in air and nitrogen.

Fig. 5: SEM images of fibre sizing distribution on (a) 871 and (b) 886 RXN cases, and (c) unsized case.
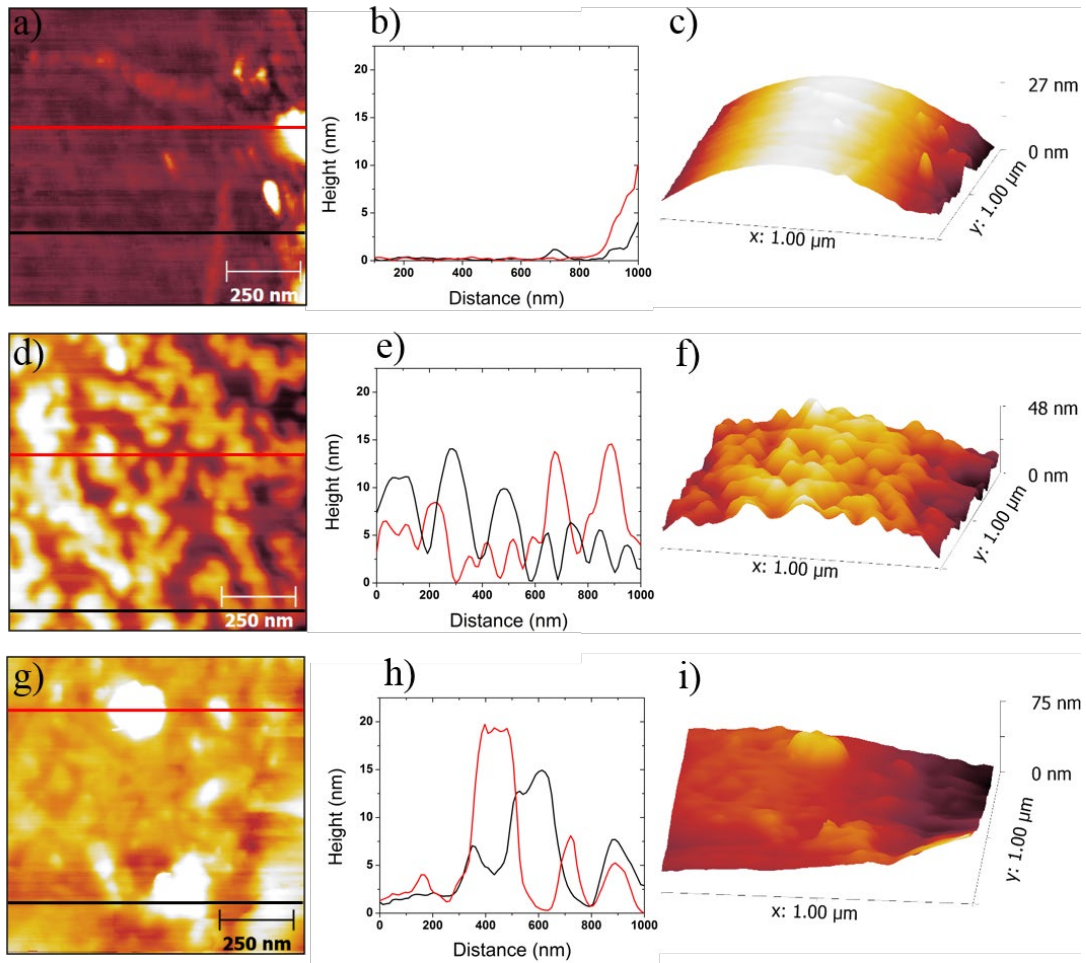
Fig. 6: Typical flattened AFM height images of each fibre type with corresponding profile plots (represented by the two horizontal lines across each image) and non-flattened 3D height images. Height images, profile plots and 3D images of the (a-c) unsized fibre, (d-f) 871 fibre and (g-f) 886 fibre.
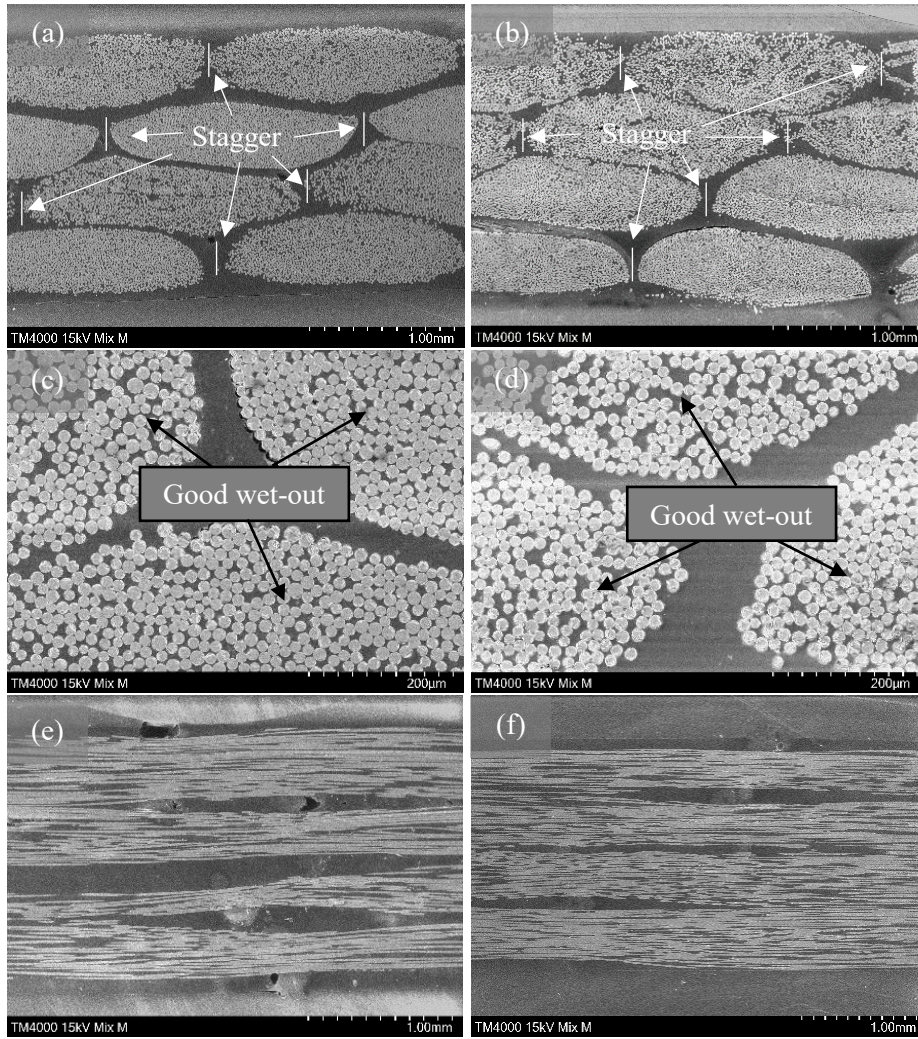
Fig. 7: SEM images of the 886 [(a), (c) and (e)] and 871 [(b), (d) and (f)] composite cases taken at surfaces perpendicular [(a), (b), (c) and (d)] and parallel [(e) and (f)] to the fibre direction.
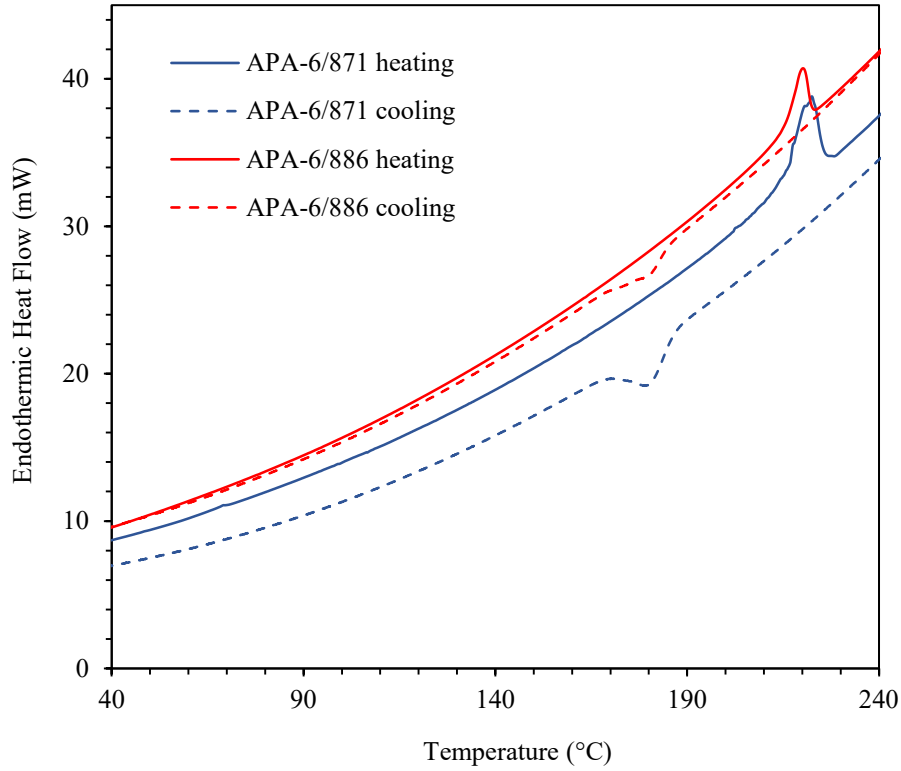
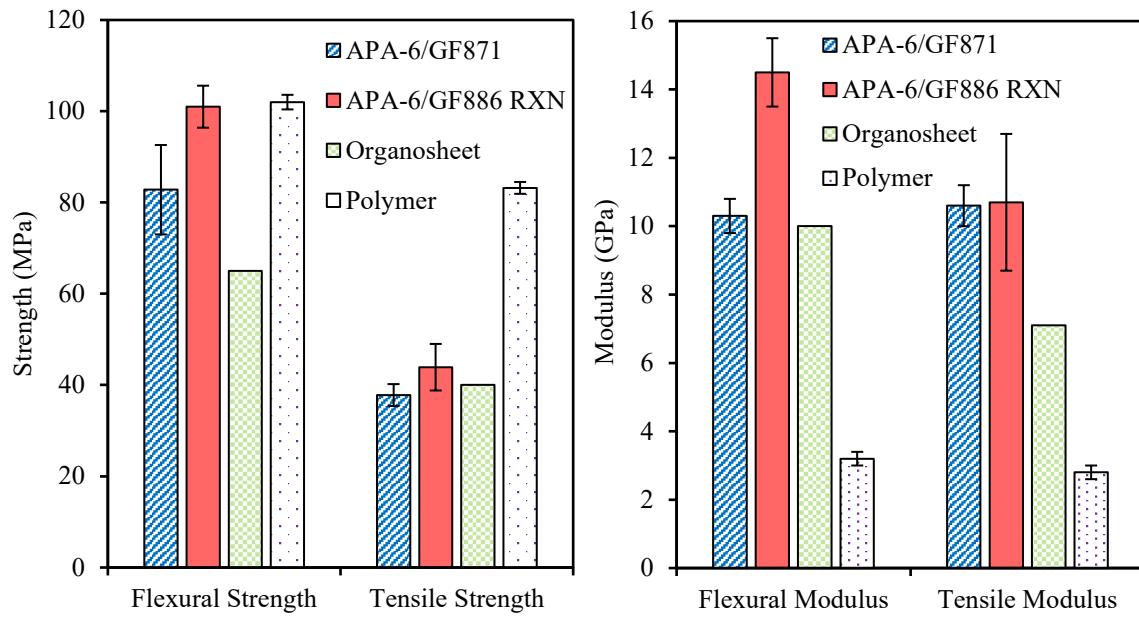**Fig. 8:** DSC curves for the 871 and 886 composites.

Fig. 9: Comparison of 871 and 886 composite transverse properties with those of the pure APA-6 matrix material and commercial organosheet given as references [32,37].

28

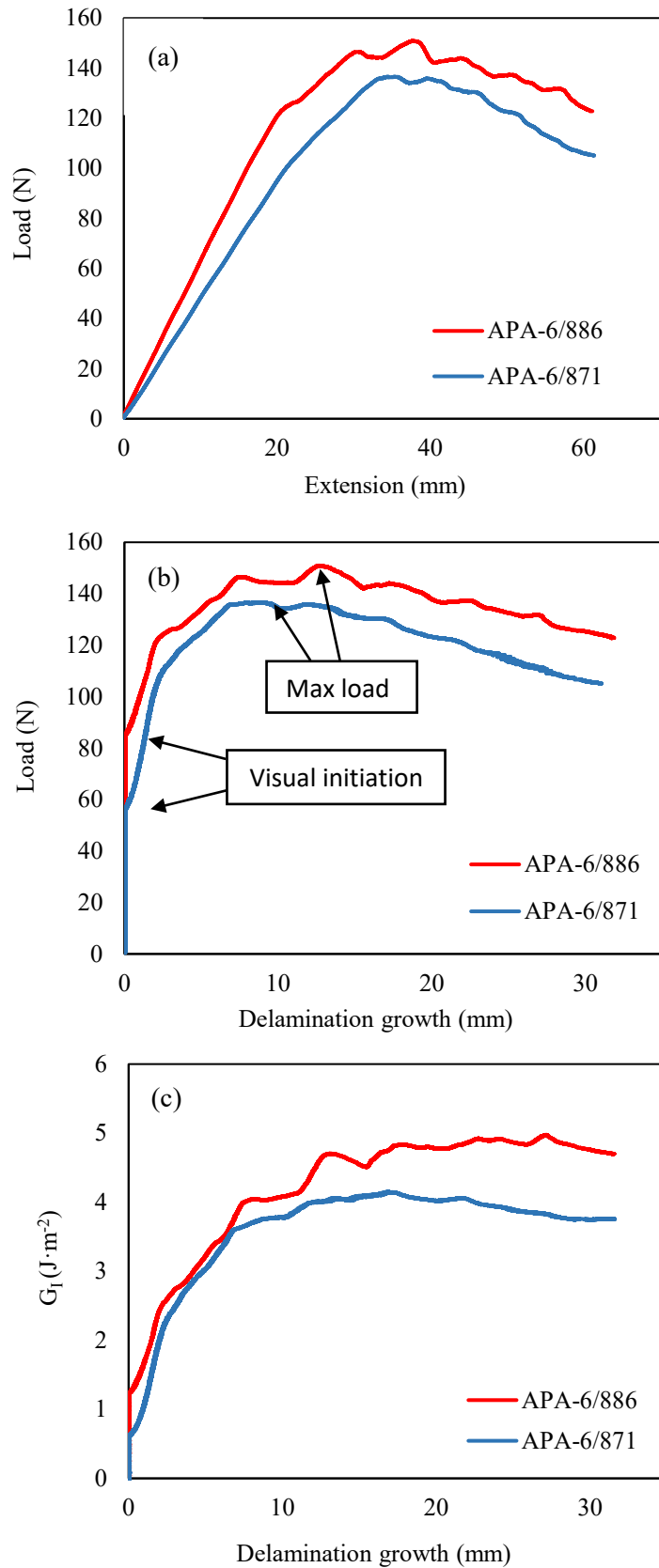**Fig. 10:** Representative DCB plots of (a) load-extension, (b) load-delamination and (c) G_I-delamination.
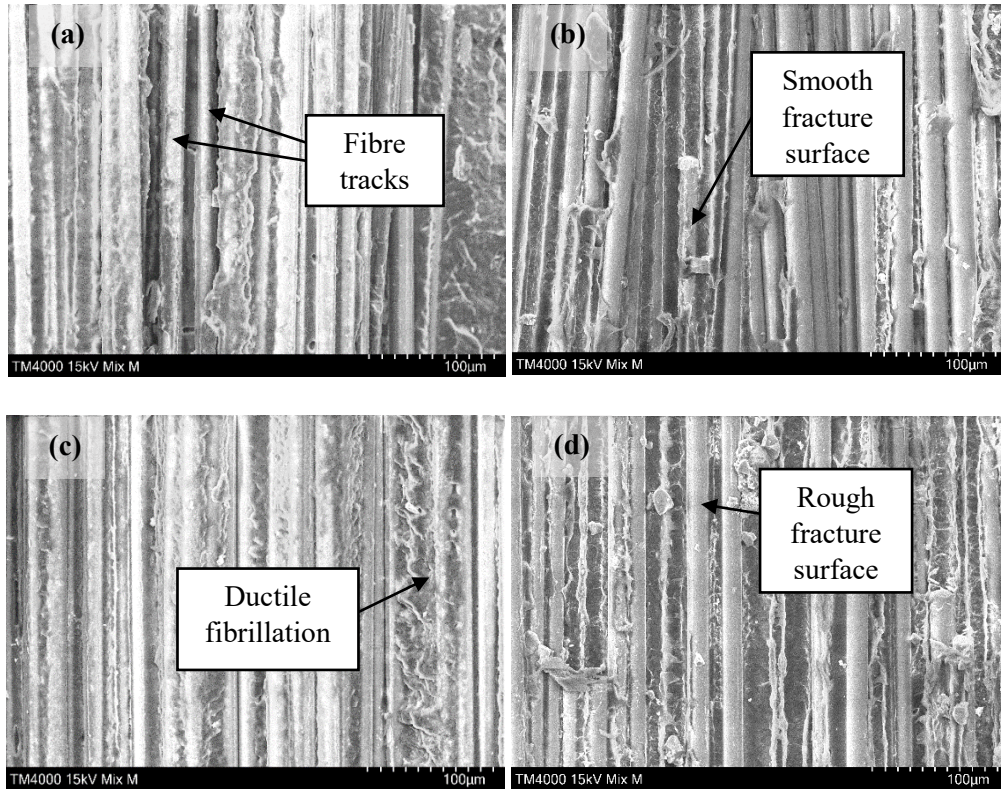
Fig. 11: SEM images of fracture surfaces of tested DCB and transverse tensile specimens for the 871 composite, (a) and (b); and the 886 composite, (c) and (d).
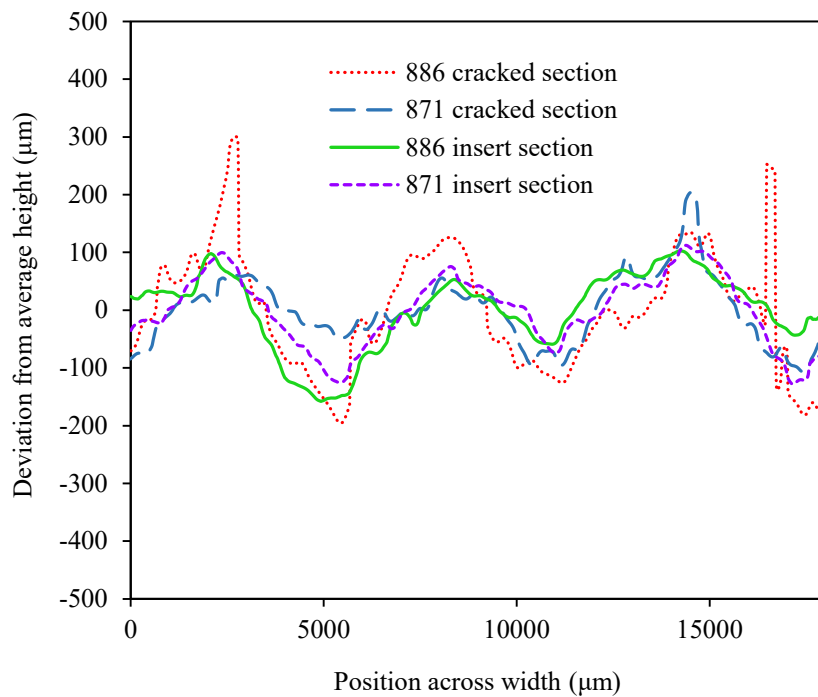

Fig. 12: Surface roughness techniques applied to stitched images at high magnifications with multi-focus image fusion.

Tables

Table 1: Mass loss determined using TGA (in air and nitrogen), burn-off and reflux.

Sizing	M_{loss} (%)			
	TGA (air)	TGA (N_2)	Burn-off	Reflux
871	0.49	0.45	0.50 ± 0.03	0.32 ± 0.11
886	0.38	0.35	0.45 ± 0.09	0.29 ± 0.15

Table 2: Quality assessment results in terms of thickness, density, and fibre volume/void fractions; and longitudinal tensile properties for the 886 and 871 composites.
*Longitudinal tensile properties have been normalised to 50% fibre volume fraction.

Material	Thickness (mm)	Density (g·cm⁻³)	Fibre volume fraction (%)	Void volume fraction (%)	Longitudinal tensile strength* (MPa)	Longitudinal tensile modulus* (GPa)
APA-6/871	1.93 ± 0.02	1.882 ± 0.025	51.8 ± 1.9	1.1 ± 0.4	1070 ± 64	39.4 ± 1.3
APA-6/886	1.86 ± 0.03	1.906 ± 0.018	53.7 ± 1.0	1.3 ± 0.6	977 ± 38	39.3 ± 1.2

Table 3: Physical properties for 871 and 886 composites.

Material	Average degree of conversion (%)	Average degree of crystallinity (%)	Melt temperature (°C)	T_g (°C)
APA-6/871	96.9	44.8	221.4 ± 0.9	85.5 ± 2.0
APA-6/886	94.9	43.3	219.8 ± 0.3	87.5 ± 2.1

Table 4: Summary of transverse mechanical properties for the 886 and 871 composites cases. Matrix properties and properties of commercially available UD glass fibre PA-6 organosheet (from bonded UD tapes) are given as a reference [19,32,37]. Shaded cells indicate a statistically significant difference between the 886 and 871 cases in accordance with Welch's t-test.

Transverse Property	Reference materials		Comparative study		Avg. % difference between 886 and 871
	Matrix [19]	Organosheet [32,37]	APA-6/GF 871	APA-6/GF 886 RXN	
Flexural strength (MPa)	102.7 ± 1.6	65	82.8 ± 9.8	99.4 ± 4.6	20
Flexural modulus (GPa)	3.2 ± 0.2	10	10.3 ± 0.5	14.4 ± 1.0	28
Flexural strain at max strength (%)	6.2 ± 0.2	-	1.09 ± 0.12	0.96 ± 0.11	-12
Tensile strength (MPa)	83.2 ± 1.3	40	37.8 ± 2.4	42.5 ± 5.1	12
Tensile modulus (GPa)	2.8 ± 0.2	7.1	10.6 ± 0.6	10.5 ± 2.0	-1
Tensile strain at max strength (%)	22.0 ± 0.5	-	0.41 ± 0.02	0.49 ± 0.08	20

Table 5: Mode I fracture toughness values for initiation by visual observation ($G_{1C\,VIS}$) and by maximum load ($G_{1C\,Max}$); and for propagation over an average range of values ($G_{1C\,Avg}$). G_{1C} values of other UD glass-fibre composites from literature are given for comparison [38,39].

G_{1C} Metric	Epoxy/GF V_f: 51.1% [38]	PA-12/GF V_f: 39% [39]	APA-6/GF 871	APA-6/GF 886 RXN	Avg. % difference between 886 and 871
$G_{1C\,VIS}$ (J/m^2)	-	1112 ± 24	1013 ± 422	1303 ± 461	29
$G_{1C\,Max}$ (J/m^2)	1377 ± 103	2655 ± 13	3527 ± 626	4005 ± 449	14
$G_{1C\,Avg}$ (J/m^2)	2048 ± 268	3147 ± 6	3684 ± 518	4037 ± 394	10

Table 6: Surface roughness values for 871 and 886 cases in terms of Ra and Rq.

Material	Ra		Rq	
	Cracked	Insert	Cracked	Insert
APA-6/871	53.2	51.3	302.5	170.8
APA-6/886	81.1	53.6	353.6	242.5